minerals

MDPI

Article

Insight into the Effect of Nanobubbles on Fine Muscovite Powder Flotation in Different Dodecylamine Concentrations and Stirring Intensities: Kinetics and Mechanism

Xinyu Zhang [1], Liuyi Ren [1,2,3,*], Shenxu Bao [1,2,3,*], Yimin Zhang [2,3,4,5], Guohao Chen [1] and Bo Chen [1,2,3]

[1] School of Resources and Environmental Engineering, Wuhan University of Technology, Wuhan 430070, China; 320884@whut.edu.cn (X.Z.); chenguohao0708@whut.edu.cn (G.C.); bochen2012@whut.edu.cn (B.C.)
[2] Key Laboratory of Green Utilization of Critical Non-Metallic Mineral Resources, Ministry of Education, Wuhan University of Technology, Wuhan 430070, China; zym126135@whut.edu.cn
[3] Hubei Key Laboratory of Mineral Resources Processing and Environment, Wuhan 430070, China
[4] State Environmental Protection Key Laboratory of Mineral Metallurgical Resources Utilization and Pollution Control, Wuhan University of Science and Technology, Wuhan 430081, China
[5] Hubei Collaborative Innovation Center for High Efficient Utilization of Vanadium Resources, Wuhan University of Science and Technology, Wuhan 430081, China
* Correspondence: rly1015@whut.edu.cn (L.R.); sxbao@whut.edu.cn (S.B.)

Abstract: Flotation-introduced nanobubbles were expected to be an efficient and economical method to recover fine muscovite. This study aimed to explore the mechanism of the change appearing in flotation after introducing nanobubbles through micro-flotation, particle vision and measurement, flotation kinetics, and induction time measurement. The results of micro-flotation, which respectively feed muscovite or muscovite pretreated with nanobubbles in different concentrations of dodecylamine (DDA), were fitted with four flotation kinetic models using Origin. Different methods were used to examine how the introduction of nanobubbles affected the flotation process. The results showed that nanobubbles improved both the flotation rate and recovery of muscovite. Nanobubbles played different roles in different stirring intensities. At low stirring intensity, nanobubbles did not perform well. In suitable stirring intensity, nanobubbles helped particles aggregate and improved the collision probability between bubbles and minerals. However, at high stirring intensity, shear forces caused by ultra-high fluid velocities could disrupt particle aggregation.

Keywords: nanobubbles; fine particle flotation; muscovite; flotation kinetics; stirring intensity

Citation: Zhang, X.; Ren, L.; Bao, S.; Zhang, Y.; Chen, G.; Chen, B. Insight into the Effect of Nanobubbles on Fine Muscovite Powder Flotation in Different Dodecylamine Concentrations and Stirring Intensities: Kinetics and Mechanism. *Minerals* **2024**, *14*, 694. https://doi.org/10.3390/min14070694

Academic Editor: Dave Deglon

Received: 12 June 2024
Revised: 26 June 2024
Accepted: 1 July 2024
Published: 3 July 2024

1. Introduction

Muscovite has recently become increasingly important and popular due to its extensive applicability in the paint, construction, cosmetic, electrical insulation material, and chemical industries. Muscovite mineral resources are abundant and widely distributed in non-metal deposits and tailings of metal ore [1–3]. However, the amount of sheet muscovite, which is a high-quality, easily processed ore, sharply declined due to over-exploitation in recent years [4,5]. Thus, the increasing demand for muscovite has promoted the development of flotation technology, which allowed the exploitation of the vast low-grade muscovite deposits and previously uneconomic tailing to treat [6]. Fine muscovite minerals are deeply processed to replace sheet muscovite and are widely used in many fields, especially in the coating and cosmetics industries [7–9]. Coarse muscovite particles are used as car paint admixtures, and fine muscovite is used to make cosmetics such as facial creams and eye shadow [10,11]. Now, the particle size of ore feed to flotation has become finer and finer; therefore, further exploring of more efficient fine-grained muscovite separation technology is particularly important [12].

Recently, numerous experiments have been conducted to explore more efficient collectors or optimize collector mixtures in the fine muscovite flotation process [13,14]. Molecular

dynamics is popularly used to study the adsorption mechanism of reagents on mineral surfaces, which is critical information for understanding the properties of new reagents or collector mixtures [15]. For instance, Cheng et al. [16] demonstrated that DOPA and TOPA have substantially better collectivity performance than dodecylamine (DDA). Further analysis through molecular dynamics revealed that the van der Waals force between $–NH_2$ of DOPA or TOPA and the O atom of water makes the minerals exhibit better hydrophobicity. However, these new collectors with higher performance do not solve the problem of high reagent consumption caused by fine-grained muscovite flotation. It is worth noting that fine particle flotation faces many challenges, and current research suggests two promising approaches to improve its efficiency [17–19]. Firstly, reducing the size of flotation bubbles can significantly increase the collision probability with fine particles, leading to more efficient adhesion. Secondly, increasing the number of fine particles can also improve adhesion by increasing the apparent particle size of minerals and, hence, the probability of collision with bubbles [20]. Researchers have made the exciting discovery that nanobubbles can remain stable on the surface of particles, promoting agglomeration between them. This unique property of nanobubbles provides a significant advantage for the flotation of fine-grained minerals [21]. Indeed, nanobubble flotation is fast becoming a popular method for fine particle flotation. Its cost-effectiveness and potential to improve mineral processing efficiency make it a promising solution for the industry. With more people turning their attention to this innovative technique, it is clear that nanobubble flotation is regarded as a game-changing breakthrough [22].

Flotation kinetics is a crucial tool in assessing flotation behavior and optimizing the flotation process [23]. Researchers have proposed effective flotation kinetic models to simulate mineral flotation behavior and improve the mineral separation index. However, there have been few studies on the effects of introducing nanobubbles on muscovite flotation kinetics. As the flotation rate depends on the probability of collection, which is regulated by particle size and bubble size, different particle-size minerals may lead to different kinetics [24]. Nanobubble pretreatment can agglomerate fine muscovite particles and increase their apparent size. Therefore, to better understand the mechanism of nanobubble flotation and unlock its potential for improved mineral processing efficiency, it is essential to discuss the influence of flotation kinetics.

In this research, nanobubble technology is employed as a pretreatment strategy for fine muscovite, which is the ore feed of micro-flotation. This study conducted comparative flotation experiments with and without nanobubbles and employed four flotation kinetic models to analyze the data. Additionally, the influence mechanism of nanobubbles in different DDA concentrations and stirring intensities was investigated by measuring induced time and particle vision and measurement (PVM). This study provides insights into the effect of the nanobubbles on fine muscovite flotation kinetics and contributes to the increase in the fine muscovite flotation recovery values by adjusting flotation conditions.

2. Experimental Procedure

2.1. Sample and Reagents

The high-quality raw muscovite sample used in this study was obtained from Henan Province, China. The X-ray Fluorescence analysis results of raw ore listed in Table 1 indicate that the purity (93.25%) of the sample meets the requirement of pure mineral flotation. Pure muscovite samples were ground in a ceramic-lined ball mill for 1.5 h and then classified using wet sieving, settled, and dried. Finally, the mineral sample (D90 = 17.38 μm) used for micro-flotation was obtained. The particle size characteristic curve of the sample is shown in Figure 1.

Table 1. Analysis results for the chemical composition of the raw ore/%.

SiO_2	Al_2O_3	K_2O	Na_2O	Fe_2O_3	CO_2
43.614	35.9	8.36	0.653	3.926	4.523

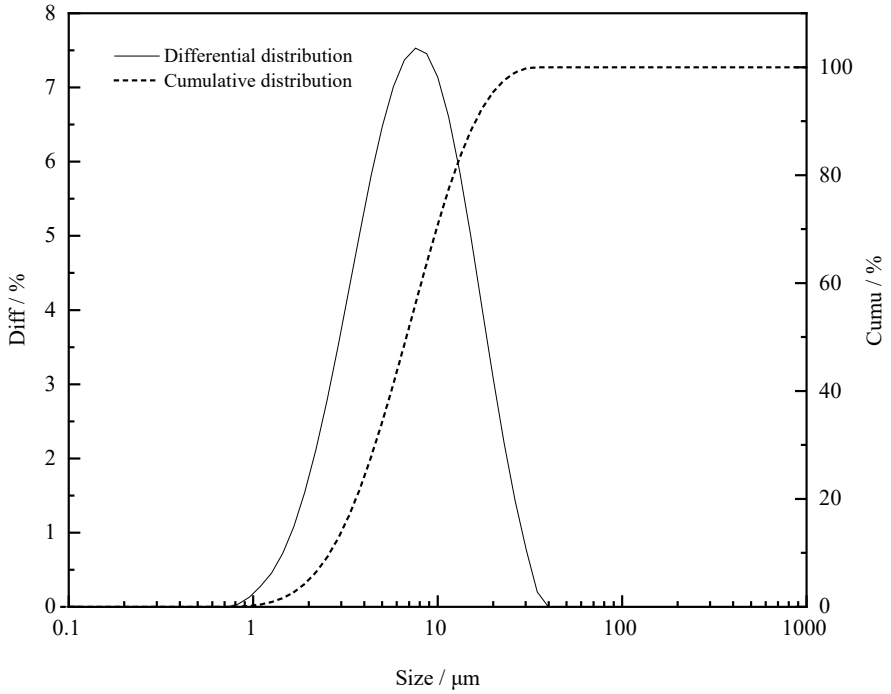

Figure 1. Particle size distribution curve of the final sample.

The cationic surfactant DDA with an analytical purity of 99.9% was purchased from Shanghai Aladdin Biochemical Technology Co., Ltd, which is located in Shanghai, China. The DDA was used as a collector in micro-flotation. NaOH and H_2SO_4, purchased from China National Pharmaceutical Group Corporation, were prepared into a 1% solution to adjust the slurry pH.

2.2. Nanobubbles (NBs)

The experiment involved using nanobubble water, generated from a nanobubble generator purchased from Yunnan Xiazhichun Company in Kunming, Yunnan province, China. The generator comprises an inlet and outlet, barometer, and box and utilizes a combination of mechanical stirring and ultrasonic cavitation to thoroughly mix the gas and liquid phases [25]. This ultimately results in the production of an aqueous solution that is rich in nanobubbles, with sizes ranging from 200 nm to 4 μm. A detailed schematic diagram of the nanobubble-generating device is provided in Figure 2, which highlights the specific components and their functions in the process.

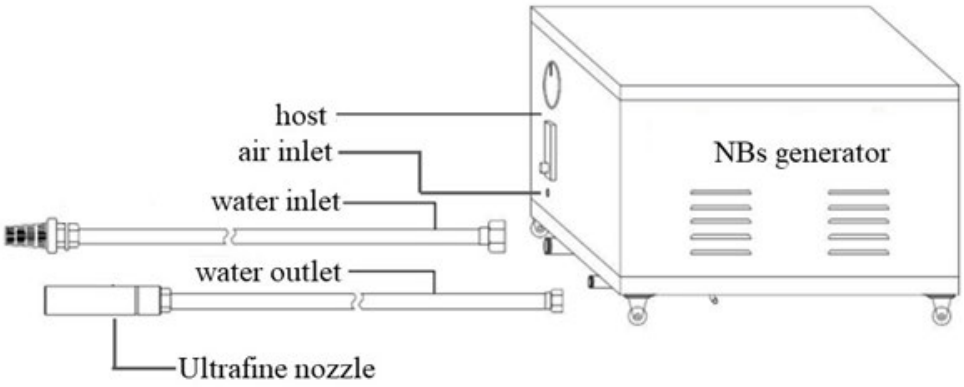

Figure 2. Schematic diagram of nanobubble-generating device.

To generate nanobubble water, ultra-pure water should be injected into the water inlet pipe with a filter hood until the water tank is filled, and the water outlet pipe with an ultra-pure water nozzle is discharged [26]. Afterward, the water inlet pipe should be inserted into the bucket with ultra-pure water, and the power supply should be switched on to start the nanobubbles generator. During operation, the ultra-pure water is drawn through the water inlet pipe, while air is sucked into the machine through the air inlet. The airflow is monitored using the flow meter control connected to the air intake. Nanobubble water is then ejected using the ultra-micro nozzle and collected with a clean beaker. The newly collected nanobubble water has a milky-white appearance. To ensure the stability of the nanobubble aqueous solution, all nanobubble aqueous solutions should be readily available. Finally, the prepared nanobubble aqueous solution can be analyzed using Zeta sizer Nano ZS 90 to determine the bubble particle size distribution in the solution, as shown in Figure 3. The Zeta sizer Nano ZS 90 was purchased from Malvern Panalytical in Shanghai, China.

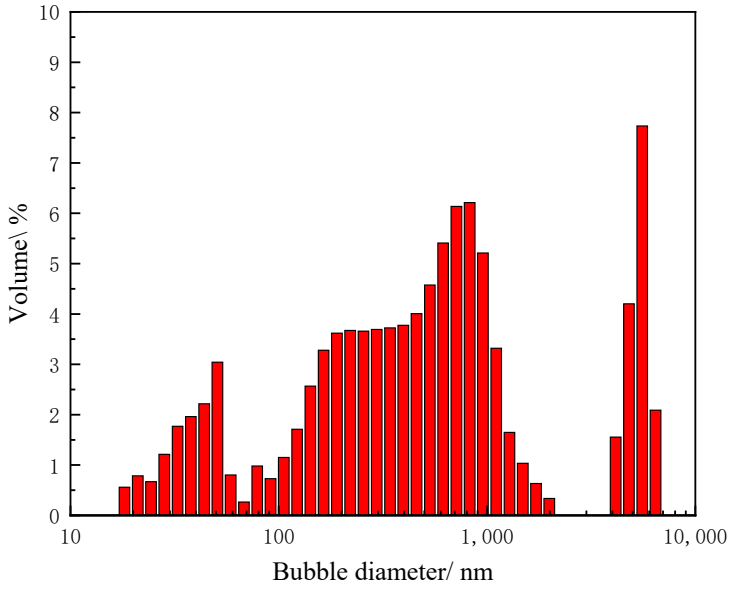

Figure 3. Bubble size distribution.

2.3. Methods

2.3.1. Micro-Flotation

As shown in Figure 4a, batch bubble scraping micro-flotation experiments were conducted using an XFGC hanging trough flotation machine, which was purchased from Jilin Prospecting Machinery Factory located in Jilin province, China. The experiment of micro-flotation was divided into the following four procedures (Figure 4b): (I) put 2 g of muscovite pure mineral in a 50 mL flotation tank, set the impeller speed at 1800 rpm, and stir for 3 min to ensure that the sample is fully dispersed in the slurry; (II) use HCl and NaOH to adjust the pH of slurry within 2 min; (III) add DDA, adjust pH, and stir for 2 min; (IV) turn on the air pump, scrape and bubble for 3 min, filter the concentrate and tailings, dry and weigh them, and calculate the flotation recovery of muscovite. For enhanced flotation by nanobubbles, the muscovite ore sample was first added to nanobubble water generated using the ultrafine rice bubble generator and stirred for two minutes. The subsequent steps were the same as the flotation process above. In this case, nanobubble water was used as supplementary water for flotation.

Figure 4c illustrates the essential flow chart for the batch bubble scraping test, a critical process that requires precision and accuracy. It is important to strictly control the scraping frequency and replace the beaker for collecting concentrate every 30 s to ensure reliable results. After 180 s, the collected concentrates and tailings were extracted and dried, and the cumulative recovery was calculated, which is crucial for obtaining accurate data.

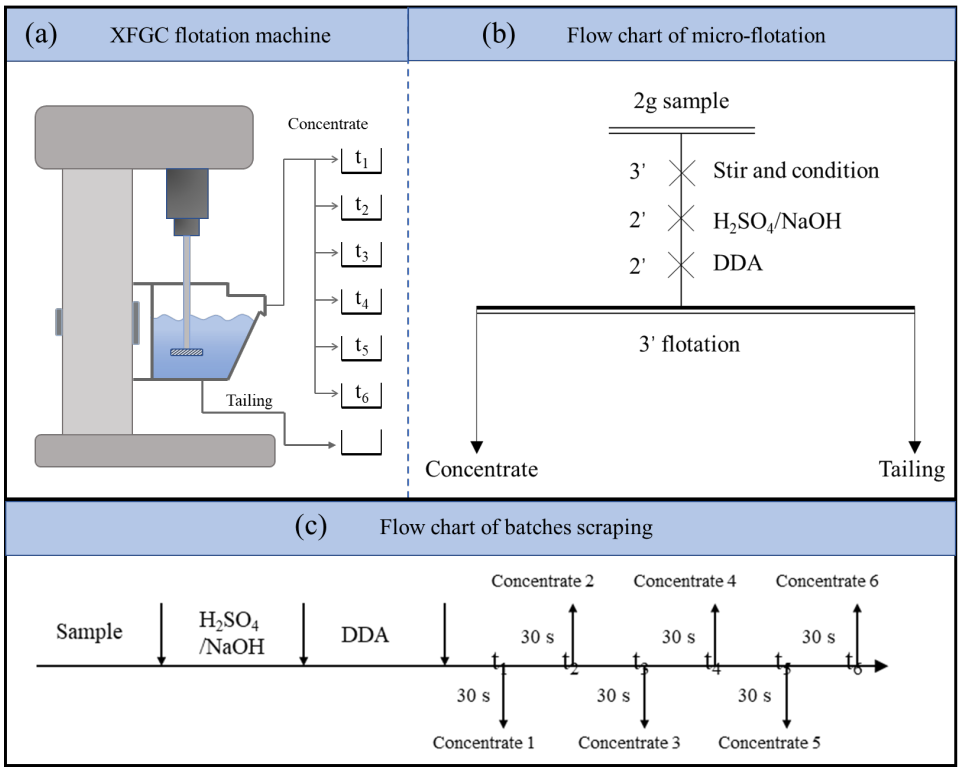

Figure 4. (**a**) XFGC hanging trough flotation machine (Jilin Prospecting Machinery Factory); (**b**) Flow chart of micro-flotation; (**c**) Flow chart of batches scraping.

2.3.2. Flotation Kinetics

Four different flotation kinetic models were applied to fit the cumulative experimental recoveries of fine-grained muscovite with defined flotation times [27,28], as listed in Table 2. The flotation kinetic parameters, including the flotation rate constant (k) and the cumulative limit recovery rate (ε_∞), as well as the four flotation kinetic formulas, were input into the Origin statistical analysis module for nonlinear analysis of the flotation data. To assess the applicability of the models, the correlation coefficient (R^2) was determined using the Origin software (2021 version), providing a robust measure of the model's suitability for the experimental data. The Origin statistical analysis module can form linear operations, nonlinear minimization, curve fitting, quadratic programming, and multi-objective programming and is a widely used data analysis software.

Table 2. Details of the flotation kinetic models used in this study.

No.	Model	Formula
1	Classical first-order model	$\varepsilon = \varepsilon_\infty\left[1 - e^{-kt}\right]$
2	First-order model with the rectangular distribution of floatabilities	$\varepsilon = \varepsilon_\infty\left\{1 - \frac{1}{kt}\left[1 - e^{-kt}\right]\right\}$
3	Second-order kinetic model	$\varepsilon = \frac{\varepsilon_\infty{}^2 kt}{1+\varepsilon_\infty kt}$
4	Second-order model with the rectangular distribution of floatabilities	$\varepsilon = \varepsilon_\infty\left\{1 - \frac{1}{kt}[\ln(1+kt)]\right\}$

Note: t—flotation time; ε—experimental recovery; ε_∞—cumulative ultimate recovery; k—flotation rate constant.

2.3.3. Particle Vision and Measurement (PVM)

The behavior of nanobubbles and mineral particles was observed using the in-situ particle vision and measurement (PVM) system [29]. 2 g sample was placed into a 100 mL breaker, and the volume of suspension was fixed at 50 mL to ensure that the slurry concentration was consistent with flotation. The probe with a high-resolution camera attached to the PVM was

then submerged under the slurry, and the height of the iron stand was adjusted to ensure that the probe was located in the center of the slurry. Magnetic stirrers were employed to replace the stirring rods of flotation machines to simulate the slurry morphology under varying stirring strengths. The magnetic stirrer speed was varied at 1000 r/min, 1500 r/min, 2000 r/min, and 2500 r/min, respectively, while the PVM probe captured images of the nanobubbles and mineral particles every 0.2 s continuously. The breaker and PVM probe were washed with deionized water, followed by ethanol, and then dried in air after each measurement.

2.3.4. Induction Time Measurement

The induction time between the muscovite flakes and the bubble was measured using a 2015EZ induction timer [30] from China University of Mining and Technology, Jiangsu. This study used two methods to measure the induction time of muscovite. One was to directly add DDA into the test sample tank and test the induction time of muscovite flakes under different solution pH; the other was to pre-place muscovite flakes in DDA solution (20 mg/L) for 30 min and test the induction time of muscovite pieces under different pH of solution. Nanobubble water was added directly to the sample tank instead of deionized water, and the muscovite mica pieces were placed at the bottom of the sample tank for 3 min, and then the induction time of the muscovite mica pieces was measured. A trapped bubble of approximately 1.3 mm in diameter was generated and fixed at the end of the bubble tube. The muscovite piece was placed at the bottom of the transparent sample cell, and the initial distance between the bubbles and the muscovite piece was set to 0.35 mm. The speed of bubbles approaching and exiting the particle bed was maintained at 2.23 cm/s. As shown in Figure 5, the bubbles remain in contact with the particle bed for a given contact time. Each experiment was repeated at specific contact times to obtain ten observations at different locations on the particle bed, and the number of observations leading to attachment was counted using a charge-coupled device (CCD) camera. To establish a distribution of induction times (seconds), the contact time is then varied by adjusting the pulse frequency. The measured value is the time at which five out of ten observations result in bubble-particle attachment.

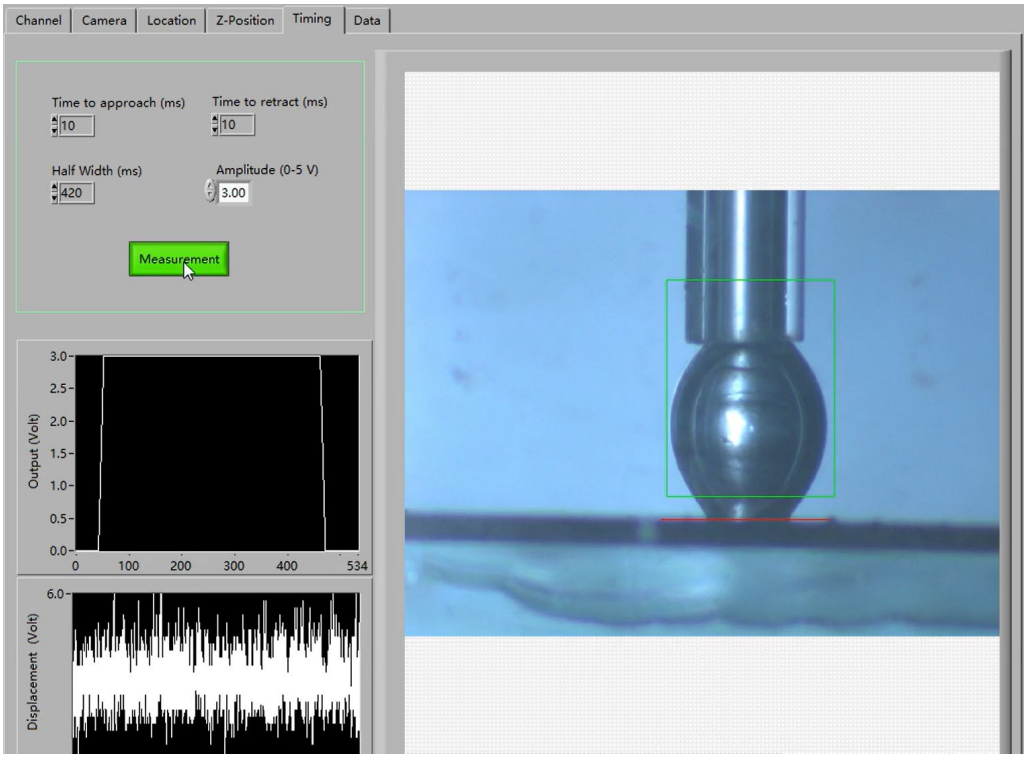

Figure 5. Bubble-particle attachment picture.

3. Results and Discussion

In the process of flotation, the study of flotation kinetics played a vital role in quantifying the influence of various conditions on flotation. It could be seen from the above conditional flotation test that the change in collector concentration, impeller speed, and the pretreatment of a nanobubble aqueous solution would lead to a change in the flotation recovery rate of fine muscovite. In order to determine the most suitable dynamic model for describing the flotation of fine muscovite and find out the change rule of the flotation rate constant itself and with various flotation factors, this section carries out the batch bubble scraping test on the flotation of fine muscovite minerals of −20 μm and uses four classical flotation kinetics models to carry out the fitting analysis of the test data.

3.1. Flotation Kinetics at Different DDA Concentrations with and without NBs

The present study investigated the effect of introducing nanobubbles on the recovery trends of fine muscovite over time, before and after nanobubbles intensification, in different concentrations of DDA. Figure 6 shows the recovery trend of muscovite before and after treatment with nanobubbles at four different DDA concentrations over time, along with their flotation kinetic fitting curves. Table 3 shows all the parameters of the flotation kinetic fitting curve. The investigation involved fitting four dynamic models to the flotation kinetics data before and after introducing nanobubbles. The results showed that the flotation rate of fine muscovite improved after nanobubbles pretreatment, as evidenced by the increased recovery from 30.85% to 38.92% for a DDA dosage of 5 mg/L. The flotation rate after strengthening did not reach the end of the flotation, while the flotation rate before strengthening had already reached the end of the flotation. The fitting results of flotation kinetics suggested that model 4 had the best-fitting effect after pretreatment. In contrast, model 1 had the best-fitting effect before pretreatment, indicating that the flotation rate of fine muscovite was improved after pretreatment. Furthermore, it was observed that the flotation effect of fine muscovite was greatly enhanced after nanobubbles were introduced for a DDA dosage of 10 mg/L. In this case, model 2 had high goodness of fit after introducing nanobubbles, while model 1 had the best goodness of fit before strengthening. Similarly, for a DDA dosage of 15 mg/L, the flotation rate was significantly improved under high agent concentration after nanobubble treatment. The fitting results showed that model 4 was suitable for the fitting after nanobubble enhancement, with the goodness of fit being the best, while model 1 still had the best goodness of fit for the flotation results before intensification. Finally, for a DDA dosage of 20 mg/L, the time to reach the flotation endpoint after nanobubble strengthening was almost the same as before without strengthening. This suggested that chemicals already dominated the flotation behavior. The kinetic fitting results indicated that model 1 had the highest fitting goodness before and after nanobubble strengthening.

It was necessary to note that by fitting the flotation kinetics of different collector dosages, the classical primary flotation kinetics model was found to be the best fit for the flotation of fine muscovite using DDA as the collector. The results showed that increasing the dosage of DDA greatly improved the flotation rate and reagent utilization efficiency, with the flotation kinetic constant gradually increasing at dosages of 5 mg/L, 10 mg/L, and 15 mg/L. However, when the dosage of DDA reached 20 mg/L, the k value began to decline, indicating that the benefit of increasing the dosage of DDA to improve the recovery effect of fine muscovite was reduced. The fitting results also showed that the introduction of nanobubbles enhanced the flotation of fine muscovite. Furthermore, the best-fitting model of nanobubbles was found to be different from that before strengthening. Overall, the fitting of the flotation kinetics equation revealed that the classical primary flotation kinetics model is suitable for describing the flotation process of fine muscovite using DDA as the collector. Finally, it was observed that the flotation effect of DDA was greatly improved by the introduction of nanobubbles.

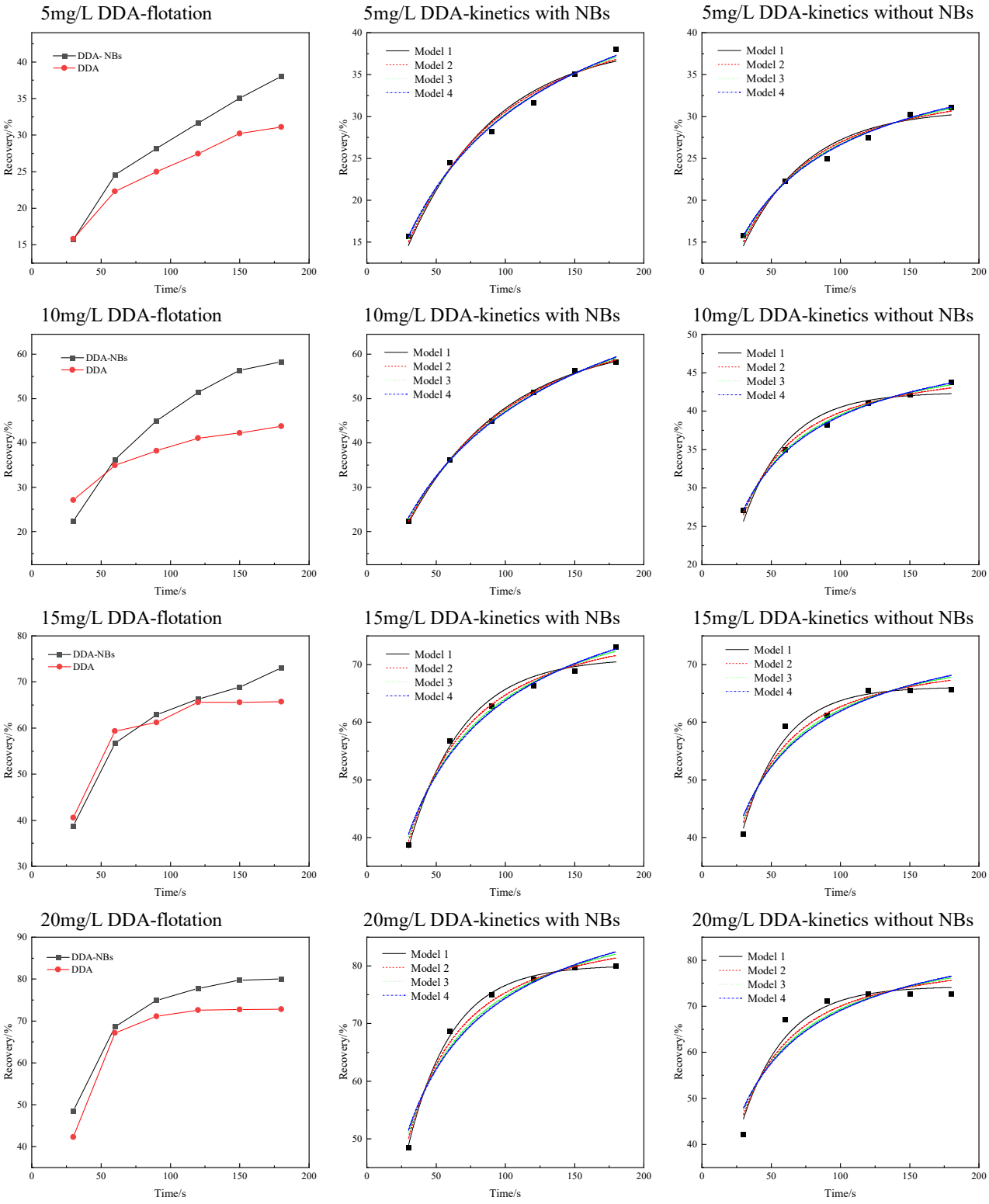

Figure 6. Recovery-time profile in different DDA concentrations with and without NBs (DDA: 5 mg/L, 10 mg/L, 15 mg/L, 20 mg/L); fitting results in different DDA concentrations with and without NBs (DDA: 5 mg/L, 10 mg/L, 15 mg/L, 20 mg/L).

Table 3. Fitting values of flotation kinetic parameters of four models at different DDA concentrations with and without NBs (DDA: 5 mg/L, 10 mg/L, 15 mg/L, 20 mg/L).

Dosage	Condition	Parameter	Model 1	Model 2	Model 3	Model 4
5 mg/L DDA	With NBs	R^2	0.977	0.985	0.991	0.993
		k	0.0156	0.0286	0.0275	0.0268
		ε_∞	38.922	45.613	51.632	58.710
	Without NBs	R^2	0.995	0.991	0.981	0.993
		k	0.0213	0.0416	0.000585	0.0452
		ε_∞	30.85	35.21	38.44	42.53
10 mg/L DDA	With NBs	R^2	0.998	0.999	0.998	0.997
		k	0.01568	0.0249	0.0137	0.0219
		ε_∞	63.39	75.34	86.75	99.84
	Without NBs	R^2	0.992	0.981	0.000801	0.979
		k	0.03094	0.0658	0.000585	0.0882
		ε_∞	42.43	46.99	49.52	0.0882
15 mg/L DDA	With NBs	R^2	0.984	0.991	0.988	0.985
		k	0.0256	0.0512	0.0336	0.0608
		ε_∞	71.187	80.325	86.21	94.05
	Without NBs	R^2	0.980	0.959	0.935	0.919
		k	0.0331	0.0702	0.000574	0.0999
		ε_∞	0.0331	73.10	76.42	81.49
20 mg/L DDA	With NBs	R^2	0.998	0.988	0.971	0.959
		k	0.0313	0.0656	0.0429	0.0896
		ε_∞	80.134	88.92	93.44	100.11
	Without NBs	R^2	0.959	0.917	0.882	0.861
		k	0.0316	0.0654	0.000465	0.0903
		ε_∞	74.34	82.64	86.68	92.79

3.2. Flotation Kinetics at Different Stirring Intensities with and without NBs

The findings of this study are presented in Figure 7, which illustrates the trend of muscovite recovery rate with time under varying impeller speeds, along with their corresponding flotation kinetics fitting curves. Table 4 provides all the parameters of the flotation kinetics curve. The results showed that when the impeller speed was set at 1000 r/min, model 1 had the highest goodness of fit, and the flotation process was still ongoing at 180 s due to the slow rotation speed of the impeller. As time progresses, the flotation rate of the ore particles decreases, and at some point, no further flotation is possible due to the agent dosage limit. The flotation recovery rate after nanobubble enhancement was lower than that without pretreatment, perhaps because the nanobubbles promoted particle agglomeration, leading to a decrease in the flotation recovery rate when the bubbles' ability to carry mineral particles was limited. At an impeller speed of 1500 r/min, the flotation recovery rate of fine muscovite remained constant before and after nanobubbles pretreatment, with model 1 having the highest goodness of fit. At 2000 r/min, the nanobubbles' strengthening effect became evident, indicating that nanobubbles can enhance flotation kinetics when the slurry speed or the amount of bubbles reaches a certain threshold. When the impeller speed was increased to 2500 r/min, the strengthening effect of nanobubbles was insignificant due to the shear force of the slurry, causing the agglomerated particles to disperse.

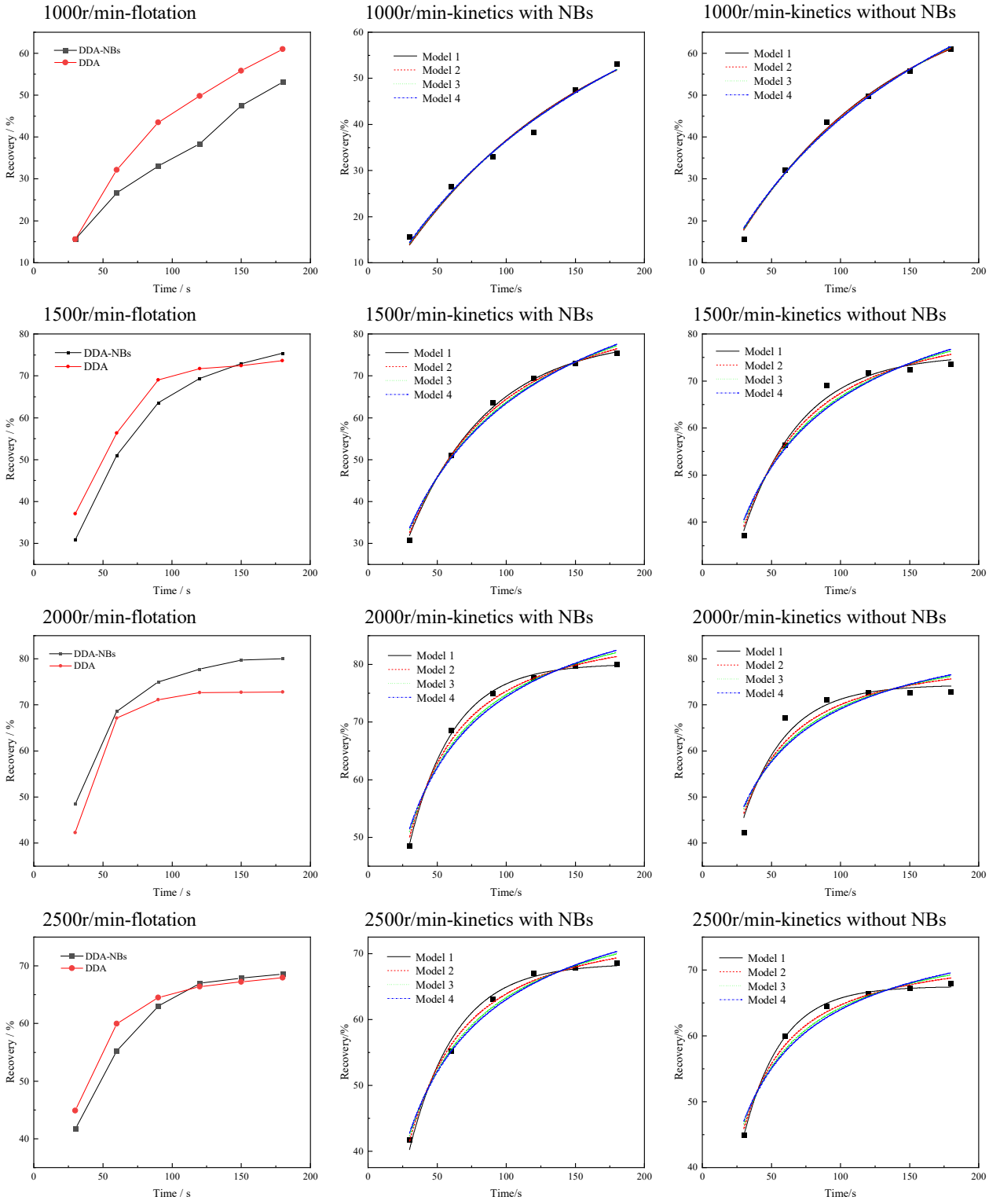

Figure 7. Recovery-time profile in different stirring intensity with and without NBs (1000 r/min, 1500 r/min, 2000 r/min, 2500 r/min); fitting results in different stirring intensity with and without NBs (1000 r/min, 1500 r/min, 2000 r/min, 2500 r/min).

The investigation of the effect of nanobubbles on the recovery trends of fine muscovite over time, before and after nanobubbles intensification, at different stirring intensities revealed important insights into the application of nanobubbles in flotation. By fitting the flotation kinetic equations of different flotation machine impeller speeds, it was concluded that the optimal

flotation kinetic model remains the same regardless of whether it is enhanced using nanobubbles or not. The classic first-order flotation kinetic model has been found to have the best-fitting goodness. The observed increase in the flotation kinetic constant k value representing the flotation rate with increasing impeller speed indicated that the flotation rate of fine-grained muscovite could be significantly improved when the flotation machine rotates at a higher speed. The strengthening effect of nanobubbles was not significant at lower or higher speeds, and the impeller speed had a significant impact on the strengthening effect of nanobubbles. It has been found that the classic first-order flotation kinetic model is suitable for describing the flotation process of fine-grained muscovite at different rotational speeds. The k value showed that the continuous increase in the flotation machine impeller speed would increase the flotation rate constant, but the final flotation recovery rate would begin to decrease at 2500 r/min. The interaction between nanobubbles and slurry flow rate could be further studied to better understand the application of nanobubbles in flotation, which has the potential to optimize the process design. These findings provided valuable insights into the potential of nanobubble-aided flotation in the recovery of fine muscovite and highlighted the importance of understanding the underlying mechanisms to improve the efficiency of the flotation.

Table 4. Fitting values of flotation kinetic parameters of four models in different stirring intensities with and without NBs (1000 r/min, 1500 r/min, 2000 r/min, 2500 r/min).

Speed	Condition	Parameter	Model 1	Model 2	Model 3	Model 4
1000 r/min	With NBs	R^2	0.992	0.983	0.985	0.986
		k	0.00718	0.0118	0.0453	0.00846
		ε_∞	71.43	88.38	109.75	132.31
	Without NBs	R^2	0.998	0.995	0.994	0.997
		k	0.0088	0.0145	0.0000527	0.0105
		ε_∞	76.75	94.86	117.02	140.45
1500 r/min	With NBs	R^2	0.998	0.994	0.987	0.983
		k	0.01717	0.0311	0.01489	0.02959
		ε_∞	79.316	92.99	104.68	118.61
	Without NBs	R^2	0.99	0.976	0.961	0.951
		k	0.02342	0.04522	0.000268	0.05116
		ε_∞	75.62	86.26	93.35	102.67
2000 r/min	With NBs	R^2	0.998	0.988	0.971	0.959
		k	0.0313	0.0656	0.0429	0.0896
		ε_∞	80.134	88.92	93.44	100.11
	Without NBs	R^2	0.959	0.917	0.882	0.861
		k	0.0316	0.0654	0.000465	0.0903
		ε_∞	74.34	82.64	86.68	92.79
2500 r/min	With NBs	R^2	0.990	0.985	0.989	0.983
		k	0.02953	0.0617	0.0459	0.08136
		ε_∞	68.482	76.196	80.465	86.568
	Without NBs	R^2	0.999	0.988	0.97	0.958
		k	0.0363	0.07995	0.000673	0.12175
		ε_∞	67.51	73.93	76.72	81.19

3.3. Behavior of Bubbles and Particles at Different Stirring Intensities with and without NBs

The results of the flotation behavior of nanobubbles and muscovite particles at different stirring speeds are presented in Figure 8. At a low stirring speed (1000 r/min), a thick deposit of muscovite appeared at the bottom of the beaker, as shown in Figure 8. The observations revealed that the incomplete distribution of muscovite mineral particles in the slurry led to reduced interaction between the particles and collector, resulting in a decreased hydrophobicity of the surface of mineral particles and a reduced probability of adhesion to bubbles. Additionally, the excessive adhesion of mineral particles to bubbles

and the formation of a thick sediment layer led to bubble overload, further reducing the muscovite recovery rate at low rotation speeds. As the stirring speed was increased to 1500 r/min, the muscovite particles pretreated with nanobubbles began to agglomerate and suspend in the slurry, possibly due to the promotion of nanobubbles [31]. However, even at 1500 r/min, a thick layer of muscovite was still deposited at the bottom of the beaker, suggesting that the nanobubble-enhanced flotation effect was insignificant at this speed. At 2000 r/min, a significant difference was observed between muscovite pretreated with nanobubbles and untreated muscovite, indicating that the stirring speed has reached an optimal level for the nanobubble-enhanced flotation recovery of muscovite ore particles. The well-defined mineral zone around a large number of bubbles that appeared and rose in the muscovite treated with micro-nanobubbles might be attributed to the promotion of agglomeration of mineral particles and the merger of bubbles by nanobubbles. This observation was consistent with the analysis results of the flotation kinetics fitting curve. At 2500 r/min, despite the presence of more nanobubbles in the pretreated muscovite slurry, mineral particles became highly dispersed due to the high shear force generated by the excessively high rotational speed. As a result, the agglomerated muscovite mineral particles bridged by micro-nanobubbles and the large bubbles produced by the merger of bubbles were broken up, thereby reducing the nanobubbles' strengthening effect. The observation of bubbles deformed by the high flow rates further confirmed the influence of shear force on the flotation behavior of muscovite particles treated with nanobubbles.

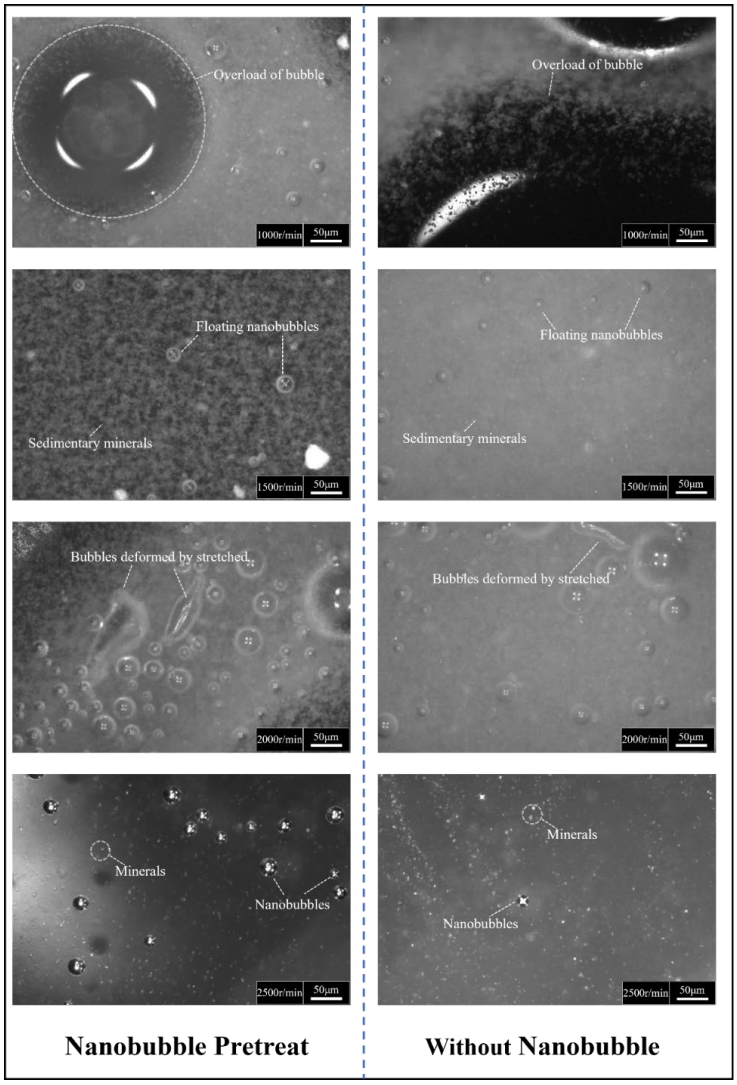

Figure 8. Images of bubble and particle behaviors at different stirring intensities with and without NBs.

3.4. Effect of Nanobubbles and DDA on Muscovite Induction Time

Figure 9 illustrates the results of the induction time measurements of muscovite flakes under different conditions. It is worth noting that the upper limit of the measurement time of the 2015EZ induction timer was 18,000 ms, and the contact time between the bubbles and the muscovite flakes was set to 18,000 ms [32]. Ten attempts were made to contact the bubbles with the mica sheets in a deionized environment. As a result, none of the bubbles adhered to the muscovite flakes. Even after pretreating the muscovite flakes with nanobubble water, the bubbles still could not adhere to the muscovite flakes, which indicated that the natural hydrophobicity of natural muscovite was weak, making it challenging for bubbles to adhere to the surface of muscovite. However, upon adding 20 mg/LDDA to the sample tank, the induction time of muscovite flakes decreased significantly, reaching the shortest time of 400 ms at pH = 4, gradually increasing as the pH of the solution increased. This phenomenon could be attributed to the electrostatic adsorption of DDA on the surface of muscovite. DDA was a cation collector, and its influential ionized cationic groups displayed an apparent regularity with the pH of the solution, appearing around the solution pH = 4 and reaching the highest level of effective group concentration of cations [33–35]. This phenomenon was previously reported by Ren et al. [36–40]. When the experimental sample was replaced with DDA-pretreated muscovite flakes, the induction time fluctuated around 400 ms with the pH of the solution, with a fluctuation range of ±20 ms, further verifying the above conclusion. After adding DDA and treating the muscovite flakes in the sample pool with nanobubble water for 3 min, the induction time of the muscovite flakes also decreased. This may be attributed to the nanobubbles pre-adsorbed on the muscovite flakes interacting with DDA. On the surface of muscovite, when the bubbles generated with the induction timer descend, they first come into contact with the nanobubbles adhering to the surface of muscovite and then merge with the bubbles, thereby increasing the adhesion probability of the bubbles and reducing the induction time of the muscovite flakes.

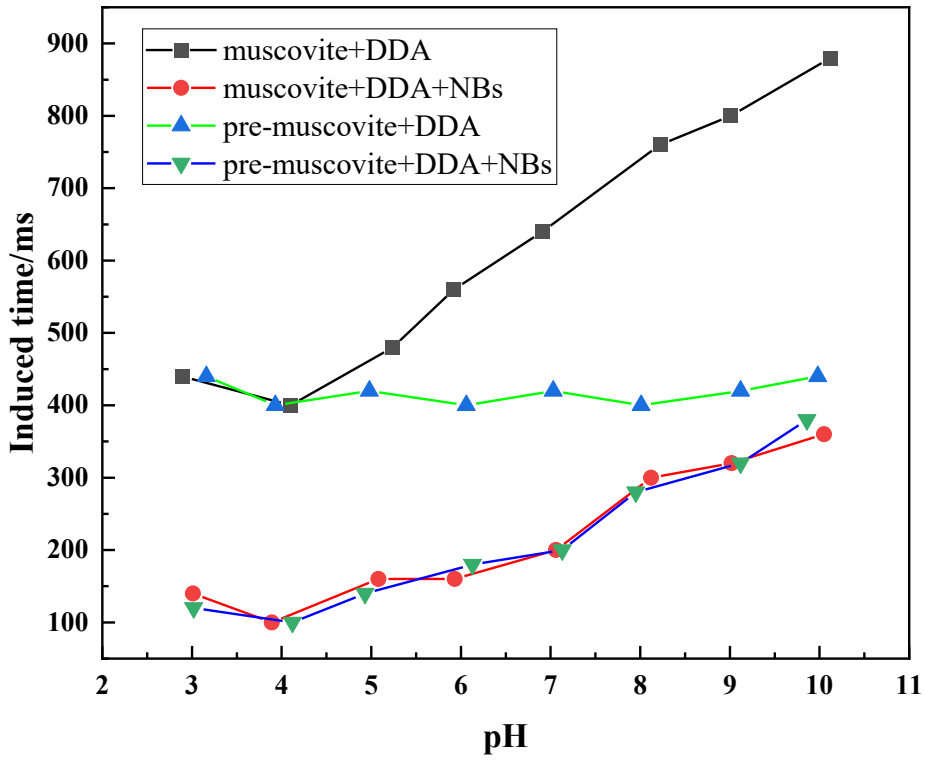

Figure 9. Induction time test results of muscovite flakes (pre-muscovite; muscovite flakes soaked in DDA solution for 30 min).

4. Conclusions

Most fine muscovite flotation studies usually ignore the effect of the basic variables of the flotation process. This study proposed to explore the influence of the basic variables essential for every flotation—agent concentration and stirring speed—on the flotation effect of nanobubble-enhanced fine-grained muscovite. The conclusions drawn are as follows:

1. The classical first-order kinetic model was consistent with the flotation of fine-grained muscovite under DDA as the collector. The flotation kinetic constant first increased and then decreased with the increase in the amount of DDA. After nanobubble strengthening, the optimal kinetic model was no longer a first-order kinetic model at low agent concentrations. Under different impeller speed conditions, regardless of whether nanobubbles enhanced it, the classic first-order kinetic model was the optimal model. At this time, the flotation kinetic constant k increases with the increase in speed, but the maximum flotation recovery rate $\varepsilon\infty$ reaches the maximum at 2000 r/min.
2. This study showed that the speed of the impeller was crucial in determining the flotation recovery rate of fine-grained muscovite. The findings indicated that the recovery rate increased as the impeller speed increased, but only up to a specific point. When the speed exceeded 2000 r/min, the recovery rate started to decline. This study also revealed that at lower speeds, the impeller's turbulent flow field was not strong enough to disperse the mineral particles in the slurry. However, the addition of nanobubbles caused the particles to agglomerate. At 2000 r/min, a well-defined mineral zone around a large number of bubbles was observed, but the large bubbles were stretched and deformed by the high speed's shear force. At 2500 r/min, the shear force broke up the mineral particles agglomerated by the micro-nano bubbles and weakened the effect of nanobubbles on the flotation of fine-grained muscovite.
3. The experimental results obtained from the induction time test indicated that the potential mechanism underlying the reinforcement of fine-grained muscovite with nanobubbles involved pre-adsorption of the bubbles onto the hydrophobic surface subsequent to their interaction with DDA. The behavior of nanobubbles and agents enhanced the probability of adhesion between large bubbles and mineral particles, resulting in a reduction in the induction time of muscovite. Such findings held significant implications for the development of efficient flotation strategies for fine-grained muscovite ores.

Author Contributions: L.R.: Experimental design, Conceptualization, Supervision, Revised the manuscript; X.Z.: Methodology, Experimental design and data collection, Investigation, Draft writing and editing, Revised the manuscript; S.B.: Funding acquisition, Project administration; Y.Z.: Project administration, Supervision; G.C.: Data collection. B.C.: Conceptualization, Supervision, Revised the manuscript. All authors have read and agreed to the published version of the manuscript.

Funding: This research was funded by the National Natural Science Foundation of China (U2003129).

Data Availability Statement: Data can be provided upon request.

Acknowledgments: The authors gratefully acknowledge the National Natural Science Foundation of China for the financial support provided.

Conflicts of Interest: The authors declare that they have no known competing financial interests or personal relationships that could have appeared to influence the work reported in this paper.

References

1. Wang, X.J.; Zhang, Y.M.; Liu, T.; Cai, Z.L. Influence of metal ions on muscovite and calcite flotation: With respect to the pre-treatment of vanadium bearing stone coal. *Colloids Surf. A Physicochem. Eng. Asp.* **2019**, *564*, 89–94. [CrossRef]
2. Marion, C.; Jordens, A.; McCarthy, S.; Grammatikopoulos, T.; Waters, K.E. An investigation into the flotation of muscovite with an amine collector and calcium lignin sulfonate depressant. *Sep. Purif. Technol.* **2015**, *149*, 216–227. [CrossRef]
3. Hosseini, S.H.; Forssberg, E. Physicochemical studies of smithsonite flotation using mixed anionic/cationic collector. *Miner. Eng.* **2006**, *20*, 621–624. [CrossRef]

4. Xu, L.; Hu, Y.; Tian, J.; Wu, H.; Wang, L.; Yang, Y.; Wang, Z. Synergistic effect of mixed cationic/anionic collectors on flotation and adsorption of muscovite. *Colloids Surf. A Physicochem. Eng. Asp.* **2016**, *492*, 181–189. [CrossRef]
5. Cloutier, J.; Piercey, S.J.; Huntington, J. Mineralogy, Mineral Chemistry and SWIR Spectral Reflectance of Chlorite and White Mica. *Minerals* **2021**, *11*, 471. [CrossRef]
6. Zhao, Z.; Li, Y.; Lei, W.; Hao, Q. Modified Graphene/Muscovite Nanocomposite as a Lubricant Additive: Tribological Performance and Mechanism. *Lubricants* **2022**, *10*, 190. [CrossRef]
7. Severov, V.V.; Filippov, L.O.; Filippova, I.V. Relationship between cation distribution with electrochemical and flotation properties of calcic amphiboles. *Int. J. Miner. Process.* **2016**, *147*, 18–27. [CrossRef]
8. Wang, L.; Sun, W.; Liu, R. Mechanism of separating muscovite and quartz by flotation. *J. Cent. South Univ.* **2014**, *21*, 3596–3602. [CrossRef]
9. Wang, L.; Hu, Y.; Liu, J.; Sun, Y.; Sun, W. Flotation and adsorption of muscovite using mixed cationic–nonionic surfactants as collector. *Powder Technol.* **2015**, *276*, 26–33. [CrossRef]
10. Wang, L.; Liu, R.; Hu, Y.; Sun, W. pH effects on adsorption behavior and self-aggregation of dodecylamine at muscovite/aqueous interfaces. *J. Mol. Graph. Model.* **2016**, *67*, 62–68. [CrossRef]
11. Rai, B.; Sathish, P.; Tanwar, J.; Moon, K.S.; Fuerstenau, D.W. A molecular dynamics study of the interaction of oleate and dodecylammonium chloride surfactants with complex aluminosilicate minerals. *J. Colloid Interface Sci.* **2011**, *362*, 510–516. [CrossRef] [PubMed]
12. Korbel, C.; Filippova, I.V.; Filippov, L.O. Froth flotation of lithium micas—A review. *Miner. Eng.* **2023**, *192*, 107986. [CrossRef]
13. Xu, L.H.; Wu, H.Q.; Dong, F.Q.; Li, W.; Wang, Z.; Xiao, J.H. Flotation and adsorption of mixed cationic/anionic collectors on muscovite mica. *Miner. Eng.* **2013**, *41*, 41–45. [CrossRef]
14. Filippov, L.O.; Filippova, I.V.; Crumiere, G.; Sousa, R.; Leite, M.M.; de Sousa, A.B.; Tripathy, S.K. Separation of lepidolite from hard-rock pegmatite ore via dry processing and flotation. *Miner. Eng.* **2022**, *187*, 107768. [CrossRef]
15. Huang, Z.; Shuai, S.; Wang, H.; Liu, R.; Zhang, S.; Cheng, C.; Fu, W. Froth flotation separation of lepidolite ore using a new Gemini surfactant as the flotation collector. *Sep. Purif. Technol.* **2022**, *282*, 119122. [CrossRef]
16. Cheng, Z.Y.Y.; Zhu, Y.M. Froth stabilities and iron ore flotation of collectors 3-dodecyloxypropanamine and 3-tetradecyloxypropylamine: An experimental and molecular dynamics study. *Colloids Surf. A Physicochem. Eng. Asp.* **2022**, *652*, 129903. [CrossRef]
17. Taguta, J.; Safari, M.; Govender, V.; Chetty, D. Investigating the Amenability of a PGM-Bearing Ore to Coarse Particle Flotation. *Minerals* **2023**, *13*, 698. [CrossRef]
18. Carelse, C.; Manuel, M.; Chetty, D.; Taguta, J.; Safari, M.; Youlton, K. The flotation behaviour of liberated Platinum Group minerals in Platreef ore under reduced reagent conditions. *Miner. Eng.* **2022**, *190*, 107913. [CrossRef]
19. Safari, M.; Hoseinian, F.S.; Deglon, D.; Leal Filho, L.; Pinto, T.S. Impact of flotation operational parameters on the optimization of fine and coarse Itabirite iron ore beneficiation. *Powder Technol.* **2022**, *408*, 117772. [CrossRef]
20. Hassanzadeh, A.; Safari, M.; Hoang, D.H.; Khoshdast, H.; Albijanic, B.; Kowalczuk, P.B. Technological assessments on recent developments in fine and coarse particle flotation systems. *Miner. Eng.* **2022**, *180*, 107509. [CrossRef]
21. Wang, L.; Sun, W.; Hu, Y.H.; Xu, L.H. Adsorption mechanism of mixed anionic/cationic collectors in Muscovite–Quartz flotation system. *Miner. Eng.* **2014**, *64*, 44–50. [CrossRef]
22. Gautam, S.; Jameson, G.J. The detachment of particles from bubbles at various locations in a turbulent flotation cell. *Miner. Eng.* **2019**, *132*, 316–325. [CrossRef]
23. Lammers, K.; Smith, M.; Carroll, S.A. Muscovite dissolution kinetics as a function of pH at elevated temperature. *Chem. Geol.* **2017**, *466*, 149–158. [CrossRef]
24. Anderson, C.; Struble, A.; Whitmore, J.H. Abrasion resistance of muscovite in aeolian and subaqueous transport experiments. *Aeolian Res.* **2017**, *24*, 33–37. [CrossRef]
25. Zhang, Z.; Ren, L.; Zhang, Y. Role of nanobubbles in the flotation of fine rutile particles. *Miner. Eng.* **2021**, *172*, 107140. [CrossRef]
26. Ren, L.Y.; Zhang, Y.M.; Qin, W.Q.; Bao, S.X.; Jun, W.A.N.G. Collision and attachment behavior between fine cassiterite particles and H2 bubbles. *Trans. Nonferrous Met. Soc. China* **2014**, *24*, 520–527. [CrossRef]
27. Zhang, X.L.; Han, Y.X.; Sun, M.; Li, W.H.; Li, Y.J.; He, J.C. Insight into the effects of grinding media on the flotation kinetics of chalcopyrite. *Adv. Powder Technol.* **2022**, *33*, 103860. [CrossRef]
28. Yianatos, J.; Vallejos, P. Challenges in flotation scale-up: The impact of flotation kinetics and froth transport. *Miner. Eng.* **2024**, *207*, 108541. [CrossRef]
29. Li, Q.; Liang, L.; Hu, P.F.; Xie, G.Y. Contribution of friction to the heterocoagulation between coal surface and quartz particles studied by the particle vision and measurement (PVM). *Colloids Surf. A Physicochem. Eng. Asp.* **2021**, *626*, 127078. [CrossRef]
30. Zhou, Y.; Albijanic, B.; Panjipour, R.; Wang, Y.L.; Yang, J.G. Understanding of attachment efficiency and induction time between bubbles and pyrite particles in flotation. *Adv. Powder Technol.* **2021**, *32*, 424–431. [CrossRef]
31. Maoming, F.A.N.; Daniel, T.A.O.; Honaker, R.; Zhenfu, L.U.O. Nanobubbles generation and its applications in froth flotation (part IV): Mechanical cells and specially designed column flotation of coal. *Min. Sci. Technol.* **2010**, *20*, 641–671.
32. Xing, Y.W.; Xu, M.D.; Guo, F.Y.; Luo, J.Q.; Zhang, Y.F.; Cao, Y.J.; Gui, X.H. Role of different types of clay in the floatability of coal: Induction time and bubble-particle attachment kinetics analysis. *Powder Technol.* **2019**, *344*, 814–818. [CrossRef]
33. Wei, Q.; Feng, L.; Dong, L.; Jiao, F.; Qin, W. Selective co-adsorption mechanism of a new mixed collector on the flotation separation of lepidolite from quartz. *Colloids Surf. A Physicochem. Eng. Asp.* **2021**, *612*, 125973. [CrossRef]

34. Fan, M.; Tao, D.; Zhao, Y.; Honaker, R. Effect of nanobubbles on the flotation of different sizes of coal particle. *Min. Metall. Explor.* **2013**, *30*, 157–161. [CrossRef]
35. Calgaroto, S.; Wilberg, K.Q.; Rubio, J. On the nanobubbles interfacial properties and future applications in flotation. *Miner. Eng.* **2014**, *60*, 33–40. [CrossRef]
36. Chen, G.; Ren, L.; Zhang, Y.; Bao, S. Improvement of fine muscovite flotation through nanobubbles pretreatment and its mechanism. *Miner. Eng.* **2022**, *189*, 107868. [CrossRef]
37. Ren, L.; Zeng, W.; Nguyen, A.V.; Ma, X. Effects of bubble size, velocity, and particle agglomeration on the electro-flotation kinetics of fine cassiterite. *Asia-Pac. J. Chem. Eng.* **2019**, *14*, e2333. [CrossRef]
38. Ren, L.; Zhang, Z.; Zeng, W.; Zhang, Y. Adhesion between nanobubbles and fine cassiterite particles. *Int. J. Min. Sci. Technol.* **2023**, *33*, 503–509. [CrossRef]
39. Ding, W.; Bao, S.X.; Zhang, Y.M.; Xin, C.F.; Chen, B.; Li, J.; Liu, B.; Xia, Y.F.; Hou, X.C.; Xu, K.H. Sustainable regeneration of high-performance cathode materials from spent lithium-ion batteries through magnetic separation and coprecipitation. *J. Clean. Prod.* **2024**, *438*, 140798. [CrossRef]
40. Rulov, M. Limitations of the Nano-Bubbles Application for Beneficiation of Fine and Ultrafine Particle Flotation. *J. Miner. Mater. Sci.* **2024**, *5*, 1–4. [CrossRef]